

Cancer model

• Liver metastasis I

H. Suemizu, M. Monnai, Y. Ohnishi, M. Ito, N. Tamaoki, and M. Nakamura. 2007. Identification of a key molecular regulator of liver metastasis in human pancreatic carcinoma using a novel quantitative model of metastasis in NOD/SCID/gammacnull (NOG) mice. *Int J Oncol* 31:741-51.

We developed a reliable new model system for assaying liver metastasis using NOD/SCID/ γ_c ^{null} (NOG) mice. Seven human pancreatic cancer cell lines were examined for their ability to form diverse metastatic foci in the livers of NOD/SCID and NOG mice. Capan-2 and PL45 showed no metastasis when seeded at up to 10^5 cells in both strains, and no BxPC-3 metastasis was observed in NOD/SCID mice. The NOD/SCID mice model could detect liver metastasis only in the AsPC-1 cell line when inoculated with more than 10^3 cells. In contrast, when inoculated with only 10^2 MIA PaCa-2, AsPC-1 and PANC-1 cells, liver metastasis was evident in 71.4% (5/7), 57.1% (4/7) and 37.5% (3/8) of the NOG mice, respectively. Capan-1 and BxPC-3 cells metastasized when seeded at 10^3 cells in 50% (5/10) and in 12.5% (1/8) of the mice, respectively. Using the NOG mice model system, we established a highly metastatic cell line, liver metastasized-BxPC-3 (LM-BxPC-3), from liver metastatic foci formed by the relatively poorly metastatic parental BxPC-3 cell line. These results demonstrated the feasibility of using the quantitative metastasis model to search for and develop new anti-cancer therapies, and novel drugs against this and other key molecules.

Table 1 Liver metastasis after intrasplenic injection of human pancreatic cancer cells.

| Cell line | Cell dose (cells/head) | Number of animal with liver metastasis ^a (metastasis/total) | | Metastatic score in NOG mice | |
|------------|---------------------------|---|----------------|--------------------------------------|--|
| | | NOD/SCID | NOG | %T/L ^b (mean \pm SD) | Liver surface area ^c (mm ² , mean \pm SD) |
| MIA PaCa-2 | 1×10^4 | 0/10 (0.0%) | 10/10 (100.0%) | 60.6 \pm 13.9 | 1056.0 \pm 338.0 |
| | 1×10^3 | 0/7 (0.0%) | 5/6 (83.3%) | ND | ND |
| | 1×10^2 | 0/6 (0.0%) | 5/7 (71.4%) | ND | ND |
| AsPC-1 | 1×10^4 | 8/9 (88.9%) | 9/9 (100.0%) | 48.2 \pm 12.3 | 434.4 \pm 77.6 |
| | 1×10^3 | 2/8 (25.0%) | 8/8 (100.0%) | ND | ND |
| | 1×10^2 | 0/6 (0.0%) | 4/7 (57.1%) | ND | ND |
| PANC-1 | 1×10^4 | 0/10 (0.0%) | 8/8 (100.0%) | 26.6 \pm 11.3 | 374.0 \pm 68.5 |
| | 1×10^3 | 0/6 (0.0%) | 6/8 (75.0%) | | ND |
| | 1×10^2 | 0/7 (0.0%) | 3/8 (37.5%) | ND | ND |
| Capan-1 | 1×10^4 | 0/10 (0.0%) | 9/10 (90.0%) | 15.6 \pm 5.3 | 425.6 \pm 38.5 |
| | 1×10^3 | 0/10 (0.0%) | 5/10 (50.0%) | ND | ND |
| | 1×10^2 | 0/8 (0.0%) | 0/8 (0.0%) | ND | ND |
| BxPC-3 | 1×10^5 | 0/8 (0.0%) | 8/8 (100.0%) | ND | ND |
| | 1×10^4 | 0/8 (0.0%) | 1/8 (12.5%) | 0.0 \pm 0.0 | 409.4 \pm 37.3 |
| Capan-2 | 1×10^5 | 0/8 (0.0%) | 0/8 (0.0%) | ND | ND |
| | 1×10^4 | ND | 0/10 (0.0%) | 0.0 \pm 0.0 | 426.7 \pm 39.1 |
| PL45 | 1×10^5 | 0/8 (0.0%) | 0/8 (0.0%) | ND | ND |
| | 1×10^4 | ND | 0/10 (0.0%) | 0.0 \pm 0.0 | 395.0 \pm 36.1 |

^a Liver metastasis was evaluated 6 weeks after inoculation of 1×10^3 , 10^4 and 10^5 cancer cells, and 8 weeks after inoculation of 10^2 cancer cells. ^b All liver images showing liver metastases in response to injection of 1×10^4 cancer cells were used to calculate the percent tumor occupancy in the liver (T/L). ^c The surface area of the liver was calculated using all liver images obtained from mice that were injected with 1×10^4 cancer cells. ND, not done.

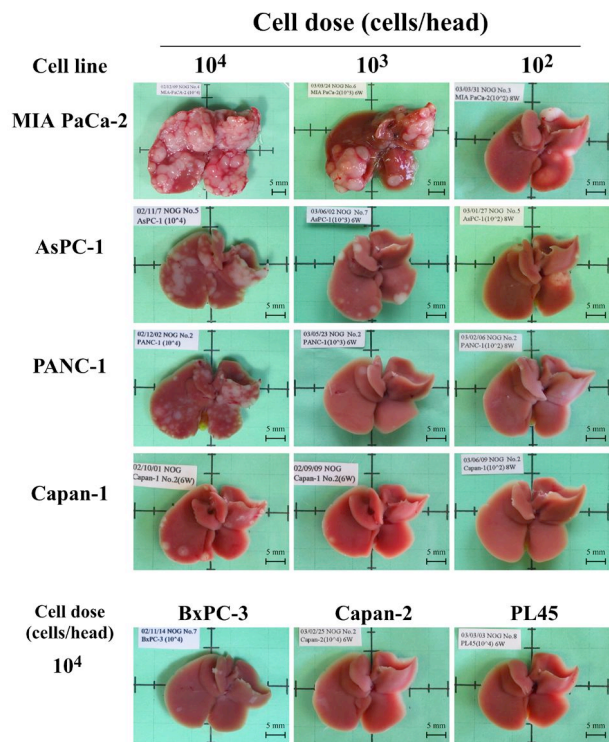


Figure 1. Representative gross findings of liver metastases of human pancreatic cancer cell lines. Seven human pancreatic cancer cell lines: MIA PaCa-2, AsPC-1, PANC-1, Capan-1, BxPC-3, Capan-2 and PL45 were intrasplenically implanted into NOG mice. The mice were sacrificed 6 weeks later, and liver metastases were enumerated immediately, without prior fixation.

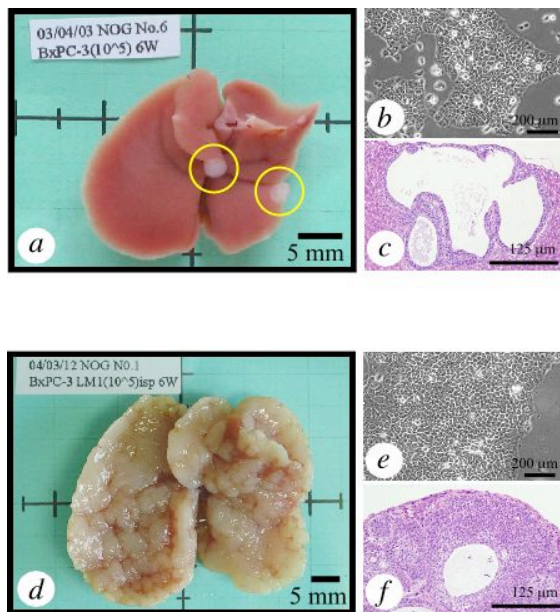


Figure 2. Establishment of a highly liver metastatic cell line. Primary tumors were generated by intrasplenic injection of 1×10^5 BxPC-3 cells into NOG mice (a-c). Cells from liver metastatic foci (open circles in Fig. 2 a) were isolated and designated as LM-BxPC-3. Metastatic ability of the LM-BxPC-3 cell line was evaluated by intrasplenic injection with 1×10^5 cells (d-f).

Cancer model

• Liver metastasis II

Hamada, K., M. Monnai, K. Kawai, C. Nishime, C. Kito, N. Miyazaki, Y. Ohnishi, M. Nakamura, and H. Suemizu. 2008. Liver metastasis models of colon cancer for evaluation of drug efficacy using NOD/Shi-scid IL2R γ null (NOG) mice. *Int J Oncol* 32:153-159.

To examine the drug efficacy of a novel farnesyltransferase inhibitor (FTI), CH4512600, *in vivo*, we developed a reliable liver metastasis model of human colon cancer using NOD/Shi-scid IL2R γ ^{null} (NOG) mice. Eleven human colon cancer cell lines were examined for their ability to form diverse metastatic foci in the livers of NOG mice as phenotypic and biological characters. When inoculated with 10⁴ COLO320DM, HCT 116, HT-29, WiDr, LoVo and LS174T cells, liver metastasis was evident in 100% (6/6), 100% (6/6), 88.9% (8/9), 87.5% (7/8), 83.3% (5/6) and 50.0% (3/6) of the NOG mice, respectively. CaCo2, COLO201, LS123, SW48 and SW1417 showed no metastasis when seeded at 10⁴ cells even in NOG mice. The mRNA expression levels and genetic mutations of *N*, *H* and *K-RAS* genes, which directly affects the levels of cellular *RAS* protein that would be molecular target for FTI, was also examined in these six metastasizable human colon cancer cell lines as molecular biological and genotypic characters. Only three cell lines had a point mutation in the *RAS* oncogene. LS174T cell line had a point mutation of the *K-RAS* gene at codon 12 (gly12 to asp; G12D), and HCT 116 and LoVo cell lines had a point mutation of the *K-RAS* gene at codon 13 (gly13 to asp; G13D). Relative gene expression levels of *N*, *H* and *K-RAS* genes in the HCT 116 cell line were 2.6 to 5.0 folds lower than that of LS174T and LoVo cell lines. We selected HCT 116 cell line from our liver metastasis model for evaluation of FTI CH4512600 efficacy in *in vivo*. Using the NOG mouse liver metastasis model, we demonstrated the effectiveness of FTI CH4512600 to suppress tumor growth *in vivo* and to prolong mouse survival significantly from 36.9 ± 2.9 to 50.3 ± 9.4 days.

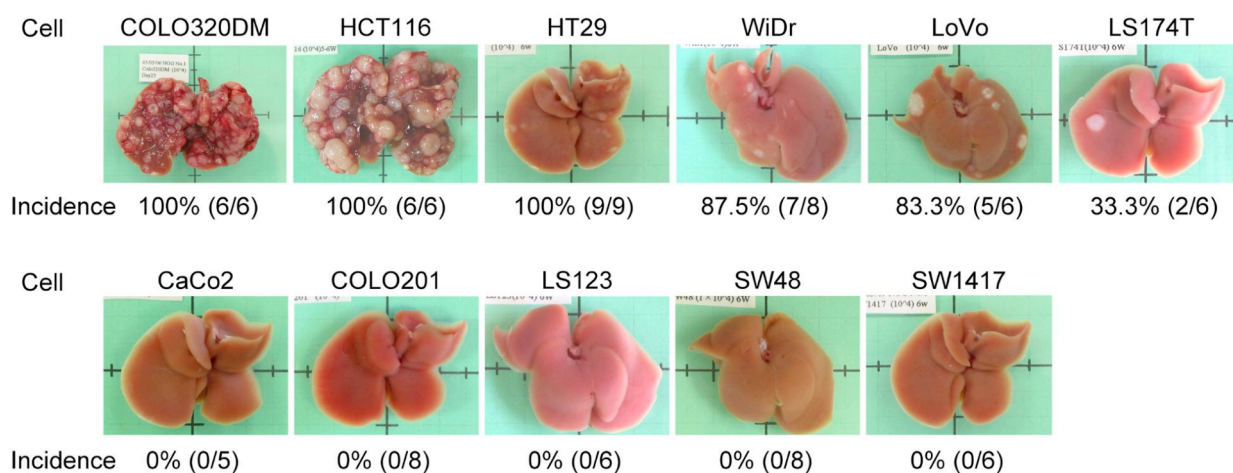


Figure1. Representative gross findings of liver metastases of human colon cancer cell lines. Eleven human colon cancer cell lines: CaCo2, COLO201, COLO320DM, HCT 116, HT-29, LoVo, LS123, LS174T, SW48, SW1417 and WiDr, were intrasplenically implanted into NOG mice. The mice were sacrificed 6 weeks later, and liver metastases were enumerated immediately, without prior fixation.

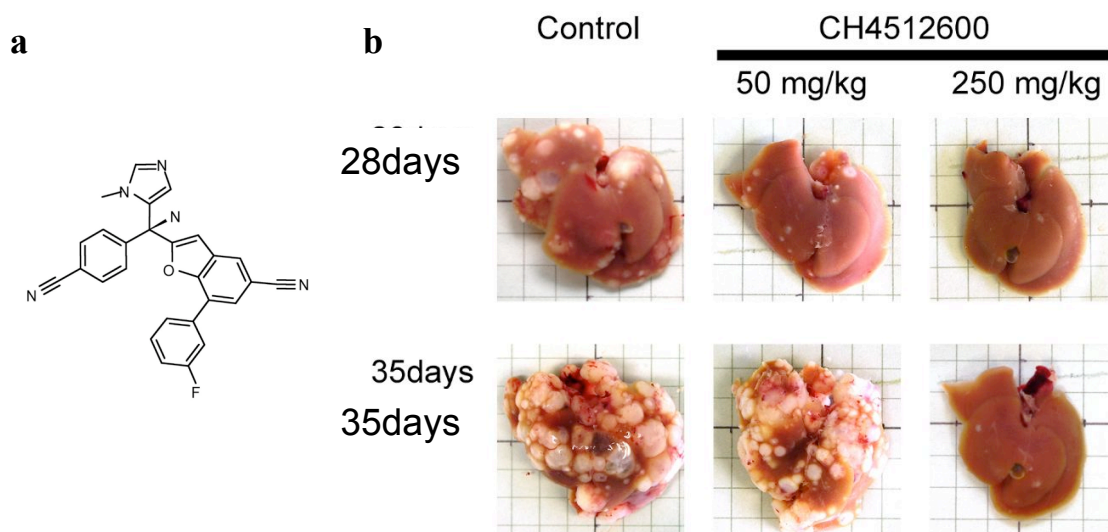


Figure 2. Effects of FTI CH4512600 on the liver metastasis model. a) Chemical structure of FTI CH4512600. b) HCT 116 cells (10^4 cells) transplanted into mouse liver was dissected at day 28 and day 35. FTI CH4512600 (50 mg/kg and 250 mg/kg, daily) was administered for 3 weeks. Representative photos are shown here (n=3).

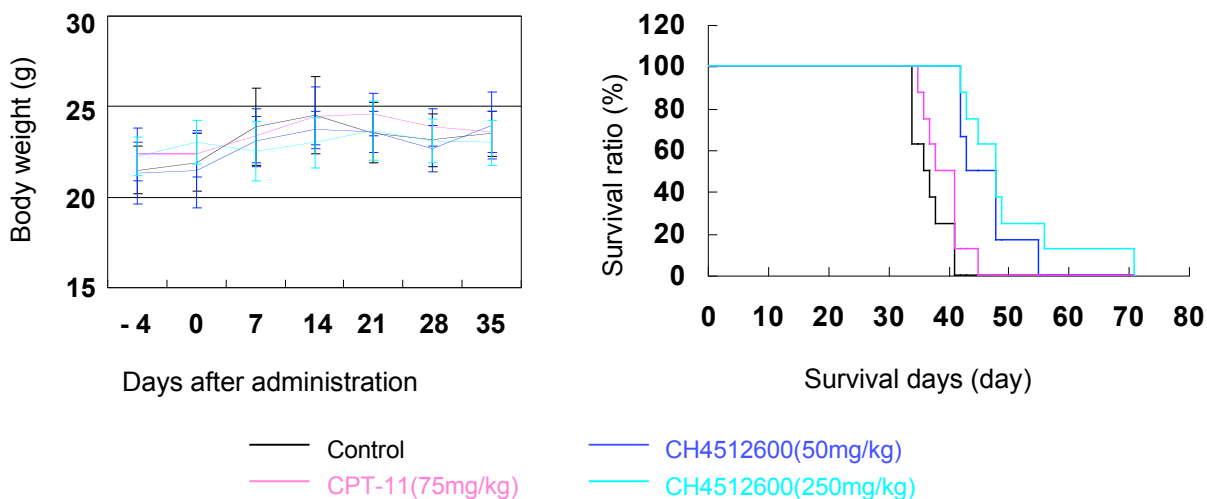


Figure 3. Body weight and survival rate of HCT 116-transplanted mice. Survival rate of HCT 116-transplanted mice for vehicle control (n=8), CH4512600 (n=8) and CPT-11-treated mice (n=6). Administration was started 3 days after the inoculation (day 0). Black line: vehicle control, blue line: CPT-11 (75 mg/kg), red line: CH4512600 (50 mg/kg), light blue line: CH4512600 (250 mg/kg). Statistical significance between control and 250 mg/kg of CH4512600 ($P < 0.0001$) and control and 75 mg/kg of CPT-11 ($P = 0.0003$) was calculated using SAS preclinical package ver.5.0.

Cancer model

• Multiple myeloma

Y. Miyakawa, Y. Ohnishi, M. Tomisawa, M. Monnai, K. Kohmura, Y. Ueyama, M. Ito, Y. Ikeda, M. Kizaki, and M. Nakamura. 2004. Establishment of a new model of human multiple myeloma using NOD/SCID/gammac(null) (NOG) mice. *Biochem Biophys Res Commun* 313:258-262.

We developed a new experimental animal model of human multiple myeloma using immunodeficient NOD/SCID/cnulle (NOG)mice. A human myeloma cell line, U266, was intravenously inoculated into 20 NOG mice, all of which developed hind leg paralysis and distress around 6 weeks after transplantation. Pathological studies showed that only the bone marrow was infiltrated with U266 cells, and no cells were present in other organs. Osteolytic lesions in cortical bones and loss of trabecular bones were prominent in U266-transplanted NOG mice. In contrast, U266 cells were not detected in CB17scid or NOD/SCID mice 6 weeks after intravenous inoculation. Human IgE, produced by U266 cells, was detected in the serum of U266-transplanted NOG mice by ELISA. The results indicated that this hu-myeloma NOG model might be useful for studying the pathogenesis of myeloma and related osteolytic lesions, and are suggestive of its applicability to the future development of new drugs.

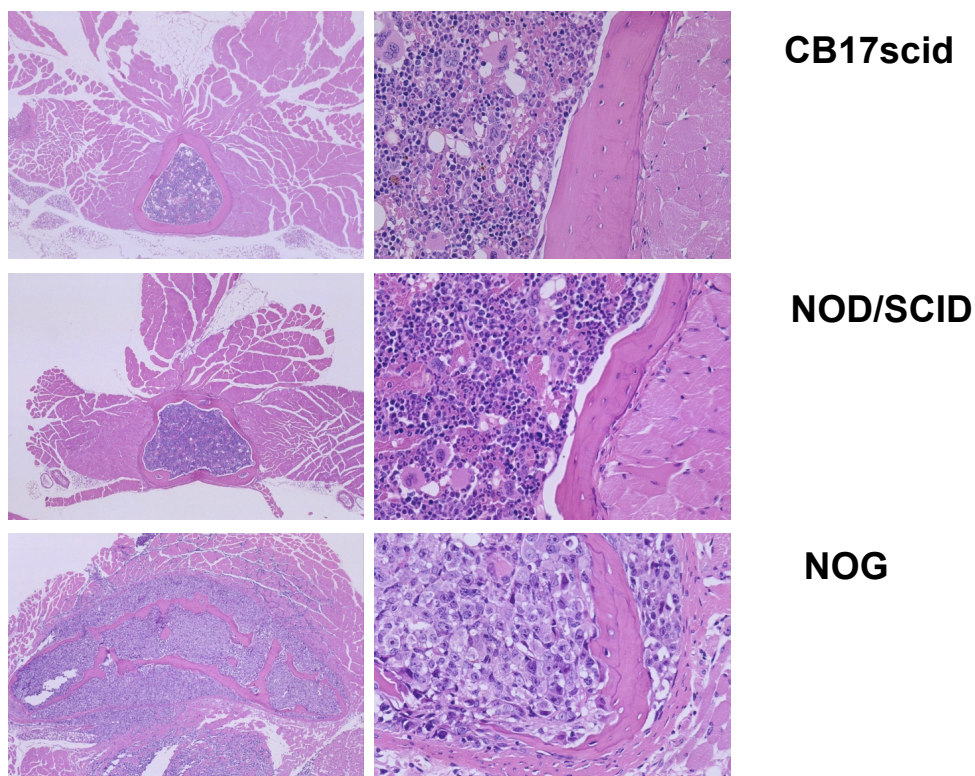


Figure 1. Histological analyses of bone marrow in CB17scid, NOD/SCID, and NOG mice after U266 myeloma cell transplantation. Five CB17scid, 5 NOD/SCID, and 20 NOG mice were intravenously injected with U266 cells after 2.4Gy irradiation. Six weeks after transplantation, all mice were sacrificed and their bone marrow from the sternum was analyzed histologically. There is no infiltration of U266 cells into the bone marrow of CB17scid (A, B) and NOD/SCID (C, D), but massive infiltration of U266 cells is observed in NOG (E, F), accompanied by osteolytic lesions (arrows in E,F). HE staining, magnification 100 x (A, C, and E), 200 x (B, D, and F).

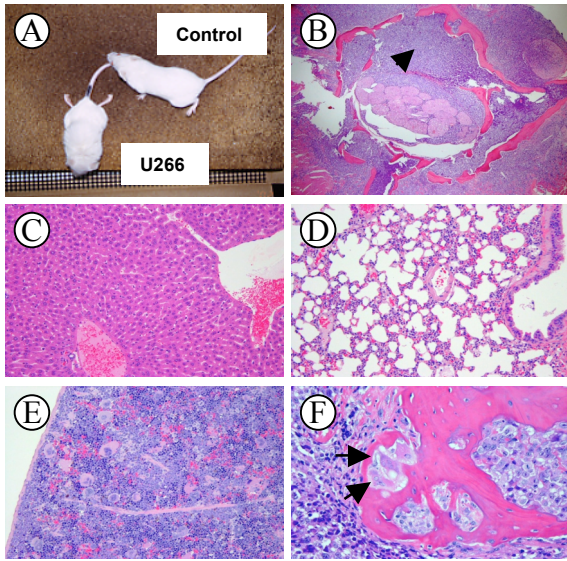


Figure 2. Clinical manifestation and histological analyses of U266-transplanted NOG mice. (A) U266-transplanted NOG mice but not control mice revealed hind leg paralysis around 6 weeks after transplantation. (B) Massive infiltration of U266 cells is observed in the lumbar bone lesions. U266 cells invade into the spinal cavity and muscles, accompanied by the osteolytic lesions. However, U266 cells are not histologically observed in other organs of NOG mice; (C) liver, (D) lungs, (E) spleen, and (F) eosinophilic osteoclasts are observed near the cortical bones of lumbar spines. HE staining.

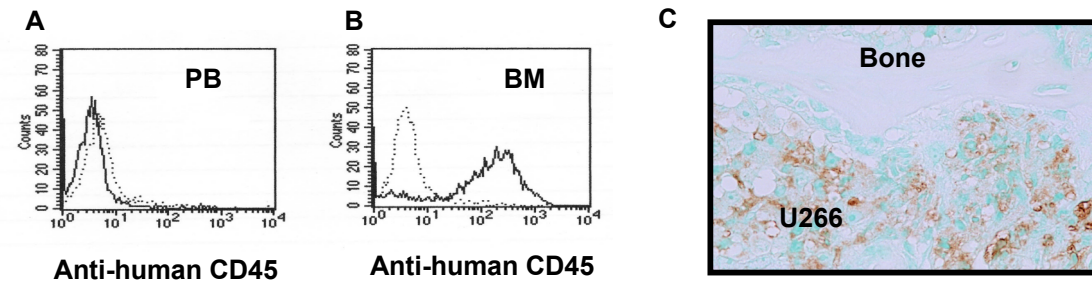


Figure 3. FACS and histological analyses of U266-transplanted NOG mice. (A) Peripheral blood of NOG mice was analyzed 6 weeks after U266 cell transplantation using a PE-conjugated anti-human CD45 antibody by FACS. Dotted lines, isotype-matched negative control. (B) Bone marrow of NOG mice was analyzed 6 weeks after U266 cell transplantation and approximately 84% was positive for human CD45. (C) Bone marrows of U266-transplanted NOG mice are stained with an anti-human IgE antibody.

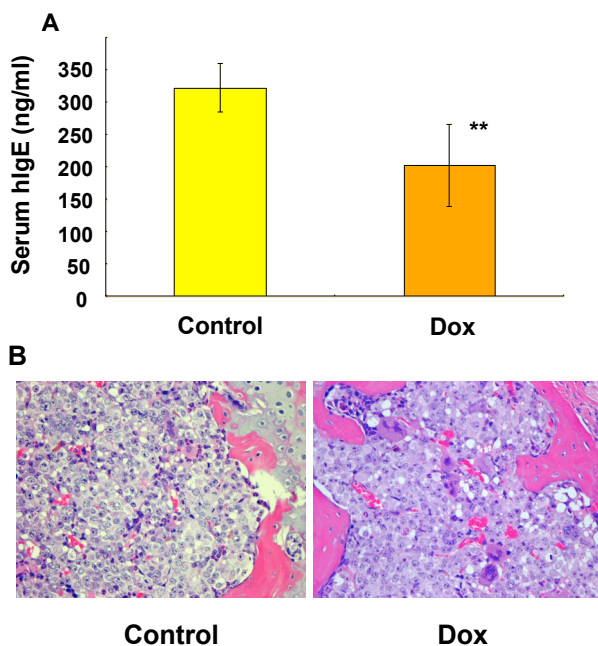


Figure 4. Serum levels of human IgE and histological studies in U266-transplanted NOG mice after treatment with doxorubicin. (A) Human IgE concentrations in serum of NOG mice 4 weeks after transplantation with U266 cells were analyzed by ELISA. Eight NOG mice were injected with 1 mg/kg doxorubicin (DOX) per day for 3 days, 1 week after transplantation (n=8). Control mice were injected with PBS in the same schedule (n=8). Values are given as means±SD of eight mice. Student's t test was performed to evaluate the statistical significances. **p < 0.01. (B) Histological studies of sternum of U266-transplanted NOG mice after treatment with or without doxorubicin in the same schedule as in (A).